Real-Time Hotspot Tracing and Model Analysis of a Distributed Optical Fiber Sensor Integrated Power Transformer

RAN DUAN

Department of Electrical Engineering, North China Electric Power University, Baoding 071003, China

Corresponding author: Ran Duan (duanran0427@163.com)

ABSTRACT With the increasing demand for electricity, overheating has gradually become a common problem for power transformers. However, the imperfect traditional monitoring method fails to detect the whole transformer in real time, which affects the safe and economical operation of the transformer. This paper was the first research utilizing a distributed optical fiber sensing system inside a running 35 kV power transformer to realize the persistent temperature monitoring of the full region. The detection accuracy of the designed winding composite sensors was also proven feasible for actual monitoring by temperature-rise tests. The hotspots were persistently traced, fluctuating at 83 %~88 %, 84 %~89 %, and 85 %~90 % of the high voltage winding height for phase A, B, and C of the 35 KV three-phase transformer, respectively. Moreover, there are multiple typical models proposed by scientists to delineate the thermodynamic behaviors of power transformers, and the hottest-spot temperature (HST) could be visualized precisely through them. In the article, the construction of four models (IEC, Swift, Susa, and IEEE models) and their comparison with the HST data from the optical fiber sensor were presented, which provided a scientific basis for seeking superior thermodynamic models. According to the evaluation of the results, the Susa model was eventually selected, which could better describe the dynamic thermal behaviors of power transformers. (RMSE was 3.0776).

INDEX TERMS Distributed optical fiber sensor, temperature monitoring, hottest-spot temperature, dynamic thermodynamic models.

I. INTRODUCTION

Power transformers are one of the most vital components in power grids. The safe operation of large transformers straightly influences the dependability and steadiness of power grids. Over time, some fault detection methods, such as dissolved gas analysis, partial discharge detection tests, etc., have been proposed to detect the operating states of transformers [1]–[3]. If a transformer works persistently without detecting the winding temperature or other aspects, the life and dependability of it will be affected, which can induce largescale power outages and other accidents. Hence, the accurate speculation of the operation status of transformers, particularly the health status of windings, can effectively reduce the probability of transformer operating failures

The associate editor coordinating the review of this manuscript and approving it for publication was Zinan Wang.

and improve the stability of power systems. Thereby, internal thermal monitoring has aroused people's interest extensively [4].

The life expectancy of a transformer directly relies on its overall insulation state which will be remarkably affected by its internal complex environment and continuously changing thermodynamic conditions. The increasing power failures induced by overheated transformer windings have evoked more and more concerns [5]–[7]. As shown in Figure 1, during the long-term operation of transformers, the short-living overcurrent circumstances (such as unexpected short-circuit, load fluctuation, etc.), which usually cause the local accumulation of heat generated from the abrupt current increase, will accelerate the high-temperature cracking of insulating materials, leading to inter-turn discharge and eventual damage to the entire winding [8]. Meanwhile, due to the uneven heating of windings, long-term overload operation or production

flaws will also result in overheated regions, reducing the thermal aging life of materials. These problems will gradually develop into weak links that affect the overall insulation of transformers. It's thus imperative to realize the internal thermal monitoring and accurate hotspot tracing for the healthy operation of power transformers.

FIGURE 1. Transformer winding breakdown caused by overheating.

Currently, the identification approaches of transformer hot spot temperature are mainly divided into the following categories: empirical formula method, numerical simulation method, and direct measurement method. Among them, the gradually matured empirical formula method has been revised many times since it was put forward in 1911, and has been extensively used in practical applications [9]. According to the IEC 60076 criterion, diverse coefficients are proposed for transformers with diverse heat dissipation methods, which can be straightly utilized for the temperature computation of hot spots under diverse load and operation circumstances [10]. However, it turns out that in some cases, the calculated results present evident errors compared with the actual measurement results [11]. At the same time, it's hard to keep up with the transient changes in load, which unavoidably causes insufficient real-time responses [12]. Hence, detection methods based on empirical formulas are more appropriate for rough and rapid calculations.

Nevertheless, the aforesaid approach merely highlights the hot spot temperature and lacks the thermal data of the entire interior region. The numeric emulation method of internal convective heat transfer partial differential equation is established based on fluid mechanics, which can solve this problem theoretically through relevant algorithms for global calculation [13], [14]. J. Smolka obtained detailed 3D thermal distributions by the combination of genetic algorithms with multi-physics coupling [15], while J. Gas-telurrutia discussed a simplified method for the heat sources and boundary conditions of oil-immersed transformers, proposing the corresponding equivalent conditions [16] for the purpose of reducing the difficulty and complexity of the 3D modeling of power transformers. Limited by the simplification of the model and the convergence of the algorithm, the numerical simulation often has deviations in reflecting the actual

transformer status, and it can only be used as a reference in most cases [17].

Direct measuring is an approach to detecting the temperature of a spot via fiber gratings, fluorescent optical fibers, thermocouples, etc. Nevertheless, there will be large monitoring blind areas due to the utilization of sensors which are unable to sense the temperature of the whole transformer. The measurement carried out by Ribeiro of A.B.L. on a 66 kV transformer in Portugal in 2008 was an extraordinary achievement[18]. Subsequently, A. Y. arranged substantial fluorescent fiberoptic sensors in the oil channel between every neighboring winding wire to detect overheated areas in a 1.5 MVA transformer [19]. However, under the influence of the complex internal environment of a transformer, different sensor positions may lead to different results.

Because of the spatiotemporally persistent monitoring and superb real-time performance [20], the distributed fiber optic sensing (DFOS) technology has been applied in many fields after decades of progress, like the kinetic monitoring of cracks and deformations in buildings or highways, since it was first put forward by Hartog in 1983 and it has displayed a remarkable potential for the application of DFOS in electrical equipment.

In the article, DFOS was utilized to continuously trace and monitor the transformer winding temperature and hotspot location, which evidenced the effectivity and stability of the designed optical fiber sensing. According to the actual structures of real transformers, diverse laying schemes have been developed for optical fibers and they have been validated by the detection accuracy assays. Through the temperature rise test of a 35kV distributed optical fiber integrated power transformer prototype, the online internal temperature under actual operating conditions was acquired spatiotemporally and persistently, and the three-dimensional visualization of the detected data was realized. The obtained data might offer a solid reference for the delicate administration of transformers. Additionally, in the past century, several classical models, like the IEC, Swift, Susa, and IEEE models, were purposed to describe the thermodynamic behaviors of transformers [21]. The prediction of the top oil temperature (TOT) and hot spot temperature (HST) by these models can help people continuously evaluate the loading capability of power transformers under different operation conditions. In this paper, these aforesaid models were established based on the principle of distributed optical fiber sensing, the results of which were compared with the optical fiber data to find the optimal model.

II. ESENTIAL PRINCIPLE
A. SENSING PRINCIPLE
When light propagates in optic fiber, due to the influence of medium molecules, light waves will encounter diverse levels of scattering, which will cause scattering spectra of different frequencies [22]. Therefore, elastic scattering (Rayleigh scattering) and non-elastic scattering (Brillouin scattering and
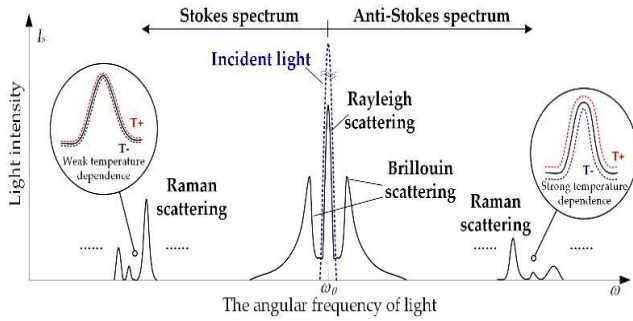
FIGURE 2. Spontaneous scattering in optical fibers.

Raman scattering) can be determined as per their frequencies (Figure2) [23]. Compared with other scattered lights, Raman scattering has been discovered to present a remarkable temperature-dependent sensitiveness, especially in its high-frequency region. Thereby, the optic fiber sensing approach was put forward.

According to relevant research [24], [25], the temperature data along the whole optic fiber can be acquired, as presented by equation (1).

$$\frac{\Phi_{AS}(T)/\Phi_S(T)}{\Phi_{AS}(T_0)/\Phi_S(T_0)} = \exp\left[-\frac{h\Delta v}{k}\left(\frac{1}{T} - \frac{1}{T_0}\right)\right] \quad (1)$$

where T_0 denotes the calibrated fiber temperature; h denotes the Planck constant ($h = 6.626 \times 10^{-34}$ J·s); Δv represents the Raman phonon frequency ($\Delta v = 1.32 \times 10^{13}$ Hz); k denotes the Boltzmann constant ($k = 1.38 \times 10^{-23}$ J·K^{-1}), and T denotes the thermal dynamic temperature. The thermal distribution along the fiber laying path can be acquired via merely identifying the electrical levels of $\Phi_{AS}(T)$, $\Phi_S(T)$, $\Phi_{AS}(T_0)$ and $\Phi_S(T_0)$ posterior to the photoelectrical conversion.

B. FOUR DYNAMIC THERMODYNAMIC MODELS
For the sake of describing the thermodynamic behaviors of transformers, certain modeling methods have been put forward, which are based on the delineation of fairly intricate thermal transference scenarios via simple differential equations. This article analyzed and compared four typical thermal models, which used the method of thermoelectric analogy, and a satisfactory result was obtained. These four models were verified via experiment outcomes, including the Loading guide (IEC) model, Swift model, Susa model, and IEEE guiding model.

1) LOADING GUIDES (IEC)
By virtue of the real-time measurement derived from the normal operation of a transformer, loading guides offer fairly simple equations for the calculation of top-oil temperature (TOT) and hotspot temperature.

Loading guides offer 2 alternatives for depicting the hotspot temperature: (a) exponential equation solution (b) difference equation solution. These methods, which have

the same source, are appropriate for arbitrarily time-varying loading factor K and time-varying environment temperature θ_a.

The former approach is actually more appropriate for the identification of thermal transference parameters by tests, particularly for product suppliers, while the latter method is more suitable for online monitoring owing to applied mathematic transformation. In principle, both methods generate identical results, as they represent solution variation due to the identical heat transfer differential equations. Therefore, we selected the latter method to establish the hot-spot model. The heat transfer differential equations are represented in the following text.

The differential equation for TOT (inputs K, θ_a, output θ_o) is:

$$\left[\frac{1+K^2R}{1+R}\right]^x \times (\Delta\theta_{or}) = k_{11}\tau_o \times \frac{d\theta_o}{dt} + [\theta_o - \theta_a] \quad (2)$$

The differential equation for hotspot temperature rise (input K, output $\Delta\theta_h$) is solved as the sum of 2 differential equation solutions, in which

$$\Delta\theta_h = \Delta\theta_{h1} - \Delta\theta_{h2} \quad (3)$$

The two equations are

$$k_{21} \times K^y \times (\Delta\theta_{hr}) = k_{22} \times \tau_w \times \frac{d\Delta\theta_{h1}}{dt} + \Delta\theta_{h1} \quad (4)$$

$$(k_{21} - 1) \times K^y \times (\Delta\theta_{hr}) = (\tau_o/k_{22}) \times \frac{d\Delta\theta_{h2}}{dt} + \Delta\theta_{h2} \quad (5)$$

The solutions of these two equations are combined as per Eq (3). The eventual equation for the hotspot temperature is

$$\theta_h = \theta_o + \Delta\theta_h \quad (6)$$

where θ_o denotes TOT (in the tank) at the load considered; θ_h denotes the winding hotspot temperature; $\Delta\theta_{or}$ denotes TOT rise in stable status at the rated losses (no-load losses + load losses); $\Delta\theta_h$, $\Delta\theta_{h1}$, $\Delta\theta_{h2}$ denote the hotspot-to-top-oil (in tank) gradient at the load considered; $\Delta\theta_{hr}$ is the hotspot-to-top-oil (in tank) gradient at rating current; θ_a is the ambient temperature; K denotes the loading factor (load current/rating current); R denotes the ratio of load losses at the rating current to no-load losses at the rated voltage; τ_o is the **o**il time constant; τ_w is the winding time constant; k_{11}, k_{21}, k_{22} is the thermal model constants.

2) SWIFT MODEL
The establishment of the Swift model started with the principle of natural thermal advection and this model offered a differential equation that considered the environment temperature for the computation of HST and TOT. In [26], [27], by virtue of thermal transference principles, Swift model has been established. The differential equations of the top oil temperature model and hotspot model are as follows.

$$D\theta_o = \frac{Dt}{\tau_{oil}} \cdot \left[\frac{I_{pu}^2\beta + 1}{\beta + 1} \cdot [\Delta\theta_{or}]^{1/n} - [\theta_o - \theta_a]^{1/n}\right] \quad (7)$$

$$\text{Minimize}: \quad \sum_{i=1}^{480} [F(\bar{x})_i - M_i]^2 \qquad (8)$$

$$D\theta_h = \frac{Dt}{\tau_{wnd,R}} \cdot \left[K^2 \cdot [\Delta\theta_{hr}]^{1/m} - [\theta_h - \theta_o]^{1/m} \right] \qquad (9)$$

where I_{pu} is the load current per unit (a forcing function variate set as 1 herein); β is the ratio of copper loss to iron loss at the rating load; τ_{oil} denotes the top oil time constant; $\tau_{wnd,R}$ is the winding time constant; m, n are exponential because of the non-linear thermal transference relationship; $F(\bar{x})_i$ denotes the TOT at every timestep as computed from (7); M_i denotes the identified TOT at every timestep.

3) SUSA MODEL

Susa in [28] offered kinetic TOT and HST models as per the principle of natural thermal advection for more precise temperature computation in instantaneous states.Moreover, he took the oil viscosity variations and loss variations with temperature into consideration. The modeling methods are as follows.

$$\frac{1 + R \cdot K^2}{1 + R} \cdot \mu_{pu}^n \cdot \Delta\theta_{oil,rated}$$
$$= \mu_{pu}^n \cdot \tau_{oil,rated} \cdot \frac{d\theta_{oil}}{dt}$$
$$+ \frac{(\theta_{oil} - \theta_{amb})^{1+n}}{\Delta\theta_{oil,rated}^n} \qquad (10)$$

$$\left\{ K^2 \cdot P_{cu,pu}(\theta_{hs}) \right\} \cdot \mu_{pu}^n \cdot \Delta\theta_{hs,rated}$$
$$= \mu_{pu}^n \cdot \tau_{wdg,rated} \cdot \frac{d\theta_{hs}}{dt}$$
$$+ \frac{(\theta_{hs} - \theta_{oil})^{n+1}}{\Delta\theta_{hs,rated}^n} \qquad (11)$$

where μ_{pu} is the oil viscosity (per-unit value); $\tau_{oil,rated}$ denotes the rated oil temporal constant; $\tau_{wdg,rated}$ denotes the rated winding temporal constant; $P_{cu,pu}(\theta_{hs})$ denotes the load loss's reliance on temperature; n is a constant set as 0.25; θ_{oil}, θ_{hs}, θ_{amb}, $\Delta\theta_{oil,rated}$, $\Delta\theta_{hs,rated}$ denote the same definition as θ_o, θ_h, θ_a, θ_{or}, θ_{hr}, respectively.

4) IEEE GUIDING MODEL

As per the principle of thermoelectrical conversion, the approach of calculating the oil temperature and winding temperature in the IEEE model does not require iteration when the load changes. At the same time, the method not only takes into account the influence of environmental temperature changes but covers the load loss and oil viscosity changes induced by resistance and oil temperature changes [29]. The models are as follows.

$$\theta_H = \theta_A + \Delta\theta_{TO} + \Delta\theta_H \qquad (12)$$

$$\Delta\theta_{TO} = \left(\Delta\theta_{TO,U} - \Delta\theta_{TO,i} \right) \left(1 - e^{-\frac{t}{\tau_{TO}}} \right) + \Delta\theta_{TO,i} \qquad (13)$$

$$\Delta\theta_H = \left(\Delta\theta_{H,U} - \Delta\theta_{H,i} \right) \left(1 - e^{-\frac{t}{\tau_W}} \right) + \Delta\theta_{H,i} \qquad (14)$$

where θ_A denotes the ambient temperature; $\Delta\theta_{TO}$ denotes the top-oil rise over environment temperature; $\Delta\theta_{TO,U}$ denotes the eventual top-oil rise over environment temperature for load L; $\Delta\theta_{TO,i}$ denotes the original top-oil rise over environment temperature for t = 0; $\Delta\theta_H$ denotes the winding hottest-spot rise over TOT; $\Delta\theta_{H,U}$ denotes the eventual winding hottest-spot rise over TOT for the load L; $\Delta\theta_{H,i}$ denotes the original winding hottest-spot rise over TOT for t = 0; τ_{TO} is the oil temporal constant of the transformer for any load L and for any specific temperature differential between the eventual top-oil rise and the original top-oil rise; τ_W is the winding temporal constant at the hotspot location.

III. DEVELOPMENT OF OIL-IMMERSED TRANSFORMER WITH BUILT-IN DOFS
A. DESIGN OF DOFS LAYING SCHEME

There are basically four types of conductors used in transformer windings: round copper conductors, flat conductors, composite conductors, and transposed conductors [30]. Round or flat copper conductors are designed for certain low current occasions, while composite conductors, made up of multiple flat wires winded in parallel, are applied in transformers with larger capacity. With a further increase in load current, transposed conductors are utilized to reduce circulating current. The high voltage (HV) winding of the 35 kV/200 kVA transformer studied in this paper had a rated current of 3.3 A and round copper wires were utilized, while the rating current of the low voltage (LV) winding was 288.7A and composite wires were utilized. In this paper, the optical fiber laying scheme on the windings of a 35 kV oil-immersed transformer is shown in Figure 3 and Figure 4.
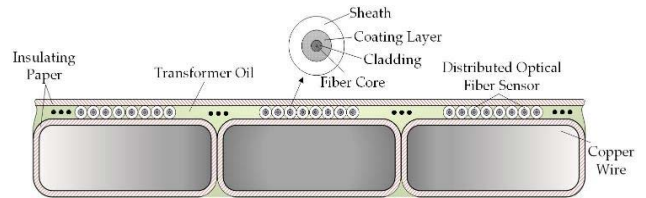

FIGURE 3. Fiber laying scheme on low voltage winding (cross-section structure).
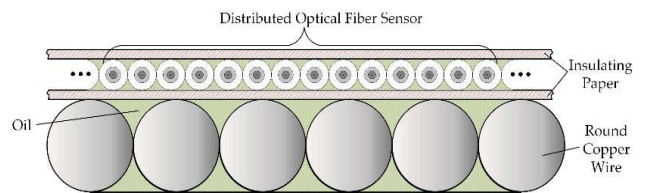

FIGURE 4. Fiber laying scheme on high voltage winding (cross-section structure).

In the laying scheme, the low-voltage winding was composed of composite conductors with the unit wound by 6 flat copper wires in parallel, leaving no oil channels between every neighboring wire (as presented in Figure 4). The high-voltage winding was composed of enameled round copper conductors, which meant less space and direct contact

between wires. For temperature sensing, optical fibers were attached to the outermost conductor surface. Additionally, to decrease the negative measurement deviation caused by the cooling medium, a tier of insulation paper was wrapped around the fiber composite winding wire. By using pulley guides, the sensor and winding wire could be highly integrated into close contact, which further synchronized the temperature of the fiber with the adjacent conductors and enabled the real-time distributed thermal monitoring along the entire winding. In the design, the distributed fiber optic sensor was wrapped between the winding wire and the insulation paper, which not only maintained the initial winding structure but buffered the possible effect of transformer oil aging (discussed in the next section).

B. STABILITY OF DISTRIBUTED OPTICAL FIBER SENSOR IN TRANSFORMER

Due to the actual requirements that optical fibers need to have satisfactory compatibility with transformer oil and work stably under high temperatures, corresponding tests were carried out in our previous work [31]. In this paper, by virtue of several materials such as Ethylene Tetrafluoroethylene (ETFE), Nylon 12, Poly Vinyl Chloride (PVC), and Polyurethane (PU), five kinds of aging characteristic indexes (water content, acid value, dielectric dissipation factor, volume resistivity, and infrared spectrum) of insulating oil were measured to study the influence of the optical fiber integrated transformer on the thermal aging characteristics of insulating oil.

Through the comparison of these parameters, ETFE exhibited the most superior comprehensive performance and was finally selected as the sheath material of the optical fiber. Figure 5 presents the aging results of four commonly used fiber materials which were shaped into dumbbells for mechanical testing.

After the 24-day aging process, the water content and acid values of the oil samples containing ETFE increased by 7.8% and 31.5%, respectively, in contrast to the pure oil samples, which were much smaller than those of the PU-containing samples (20.1% and 61.3%). Additionally, material (ETFE) still maintains a steady property posterior to the long-term aging process of the transformer oil but has no effects on its sensing performance. At the same time, the electric properties of ETFE optic fibers were eligible for the real application of transformers because of their satisfactory insulative performances. The unit 'd' in Figure 5 represents the number of test days.

C. ACCURACY OF DISTRIBUTED OPTICAL FIBER SENSOR ON TEMPERATURE DETECTION

In this paper, in order to explore the accuracy and sensitivity of distributed optical fiber sensors in transformer winding temperature measurements in a more detailed and in-depth manner, the mathematical model was established and solved by the finite element method (FEM) using the COMSOL software, and the conclusion was drawn through the analysis of calculation results.
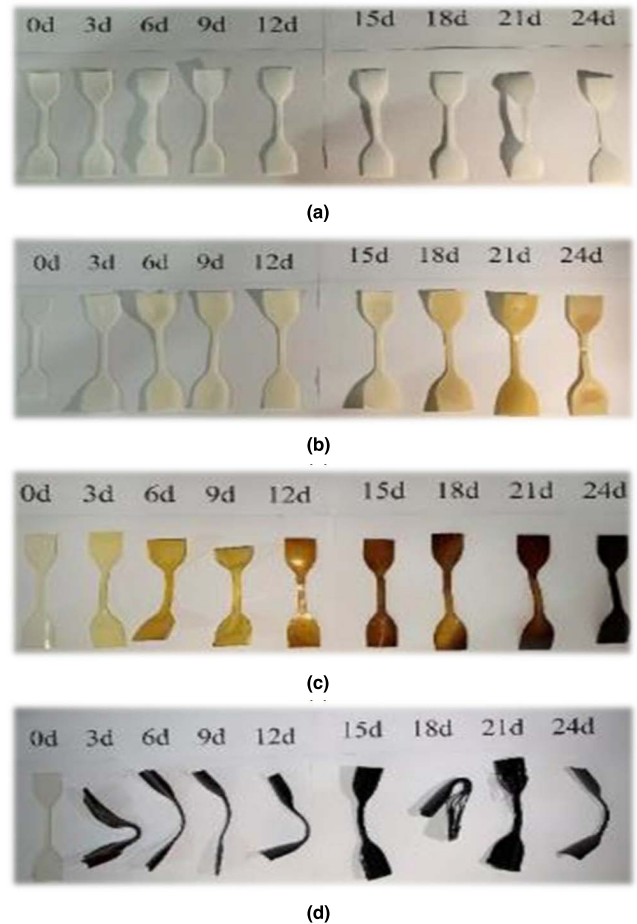

FIGURE 5. Four commonly used fiber materials during the accelerated thermal aging test: (a) ETFE; (b) Polyurethane (PU); (c) Nylon 12; (d) Poly Vinyl Chloride (PVC).

Distributed optical fiber sensors present a synchronous increase of temperature by closely attaching to the winding wire. Considering that there were multiple insulation media between the fiber core (the actual temperature sensing area) and copper wires, and that there was the effect of heat dissipation caused by the external circulating oil flow on fibers, the corresponding calculation of temperature detection efficiency was applied to the designed fiber laying scheme by virtue of the laminar flow module of COMSOL Multi-physics (5.4, COMSOL AB, Stockholm, Sweden). The entire material and mesh parameters are presented in Table 1 and Table 2, respectively.

The wire heat rate was set as 40 W, and the oil temperature was 65 °C, while the boundary conditions were set to natural convection heat dissipation coupled with a flow field to simulate the real scenarios inside the transformer. The stable distribution of thermal and flow fields is displayed in Figure 6. The mesh model and the partially enlarged view of the critical zones of the temperature distribution profile are displayed in Figure 7.

When the finite element method was used to calculate the fluid-temperature field and construct the mesh model, the

TABLE 1. Model material parameters for the thermal field simulation.

Material	Fiber Core [1]	Coating Layer	Sheath Layer	Insulating Paper	Transformer Oil	Copper Wire
Density (kg·m^{-3})	2300	1090	1000	1150	923	8940
Heat capacity [2] (J·(kg·K)$^{-1}$)	966	1970	385	1929	3639	386
Conductivity (W·(m·K)$^{-1}$)	7.60	0.12	0.11	0.25	0.21	400

[1] Containing cladding and the fiber core which was only 9 µm in diameter, and could be ignored during the thermal simulation. [2] At constant pressure.

TABLE 2. Model mesh parameters for the thermal field simulation.

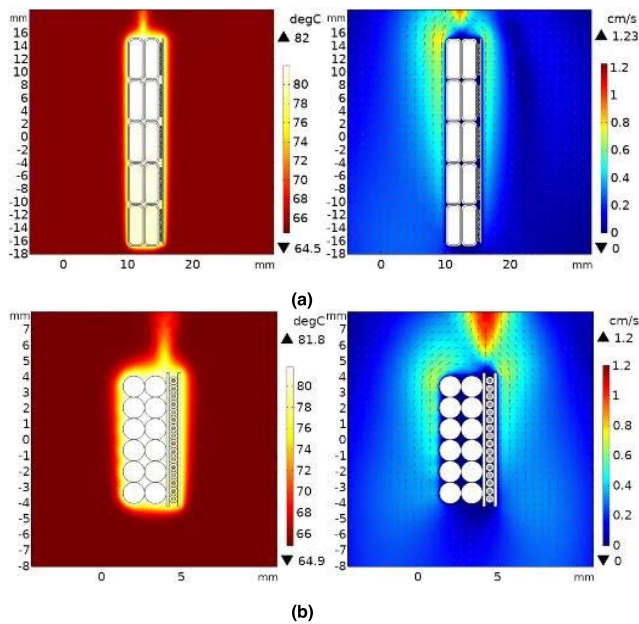| Mesh parameters	mesh vertices	units	Average unit mass	cell area ratio	grid area/mm^2
High voltage winding	23662	42472	0.7822	4.617E-7	400
low voltage winding	61109	110857	0.7838	3.203E-8	3025

FIGURE 6. Thermal simulation coupled with flow field: (a) Temperature field and flow field for LV winding; (b)Temperature field and flow field for HV winding.
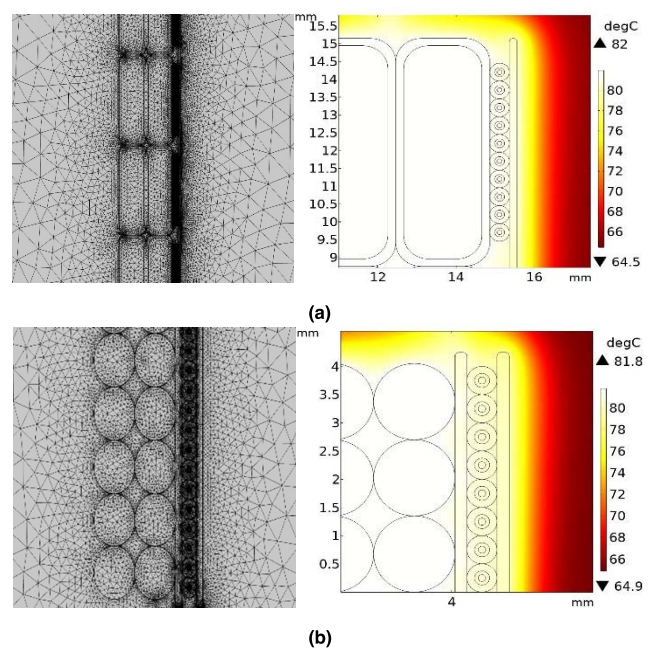

FIGURE 7. Mesh model and partial enlargement: (a) LV winding; (b) HV winding.

mesh was divided according to the field quantity distribution. If the quality of the mesh is not good, numerical oscillations may occur in the calculation, which will lead to the non-convergence of calculation results. The research showed that the larger the Pe, the clearer the numerical oscillation phenomenon of the finite element solution. Obviously, the calculation formula of Pe is shown as follows.

$$Pe = \frac{Uh}{\eta(\lambda)} \qquad (15)$$

where Pe is the Becquerel number; h is the characteristic length of the grid; η is the dynamic viscosity; λ is the thermal conductivity.

In this paper, the method of densifying the local grid was used to reduce the number of Becquerels Pe and eliminate the phenomenon of distortion oscillation. The meshing order was determined according to the size of the geometric model. During the meshing, the meshes between the part in contact with the winding and the optical fiber and the inner mesh of the fiber were refined, which could effectively improve the calculation efficiency and ensure better convergence as well as higher accuracy (Figure7). The calculation model utilized a variety of meshes, among which the fluid-structure coupling boundary was used to solve the stable boundary layer mesh, and it improved the mesh resolution and the convergence. Triangular meshes were utilized for the solid

and fluid domains, which could be readily divided and had strong adaptability to irregular areas.

The simulation only focused on the local area where the optical fiber was applied, and a short part of the entire winding was taken for the convenience of study, which would lead to a similar conclusion when we took the whole winding into the calculation. The thermal simulation result showed that for the LV winding (Figure 6(**a**)), the average temperature of the winding wire was 81.90 °C while the sensed temperature of the optical fiber (the average temperature of the core area) was 81.53 °C. The near-range temperature distribution of the optic fiber composite wire was uniform, and the heat transfer efficiency between the conductor and optical fiber was 99.55 %. For the high voltage winding (Figure 6(**b**)), the copper wire exhibited an average temperature of 81.76 °C compared to 80.82 °C of the fiber core, and the efficiency could also reach 98.85 %.

According to the flow field results, the oil flow velocity near the sensing fiber dropped to approximately 0 cm/s, which formed a relatively static area with almost zero flow and little heat loss (Figure 6(**a**) and Figure 6(**b**)). The area with the highest flow velocity (maximum value about 1.2 cm/s) appeared at the top of the winding, while the lowest velocity region emerged quite near the winding wire and the insulating paper due to the boundary layer effect. The calculation result exhibited the theoretical feasibility of distributed optical fiber sensors in identifying the real temperature of transformer windings.

Moreover, the distribution and change of the temperature field at the fiber can be seen through the partial magnification of the place where the winding and the fiber were attached (Figure7). Even though the external oil flow and insulating materials might have some influences on heat transfer, the optical fiber could still detect the exact winding temperature within an error of 1 °C. In addition to the small size of the optic fiber sensor, this could also be attributed to a relatively closed local area formed by 2 tiers of insulation paper wrapped around the optical fiber, thus, the effect of external oil flow could be limited at the greatest extent and heat could be easily transferred to the fiber core.

To further examine the temperature measurement accurateness of the proposed winding wire composite optical fiber sensor, a winding model of the 31.5 MVA/110 kV oil-immersed transformer was fabricated to perform the temperature rise experiment.

In the experiment, the distributed fiber optic sensor was fixed on the outermost circle of the winding with insulation paper. To realize temperature control, the heating tape was sampled at multiple points by thermocouples, which were closely attached to the inside of the winding wire to guarantee that the temperature control error was less than 0.5°C. Moreover, to simulate the actual heating process of an operating transformer, the windings were heated from 55°C to 75°C for 30 minutes at a gradient of 5°C to ensure that the temperature distribution reached a steady state.
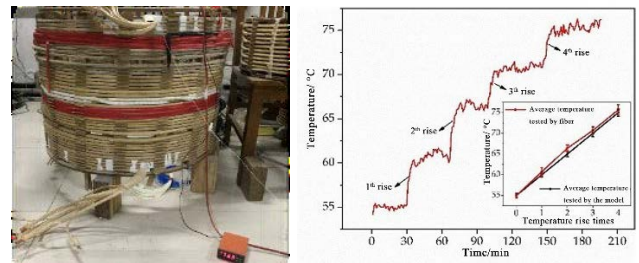

FIGURE 8. Temperature accuracy testing site and results.

The fiber measurement outcomes are presented in Figure 8. The actual assay displayed that the average temperature error of thermocouples was about 0.7 °C and that of the DOFS was approximately 1 °C. As presented in Figure 8, by excluding the systematic and accidental errors in the test, the designed winding composite fiber could accurately reflect the real temperature of the transformer winding.

The hotspot positioning accuracy was also experimentally explored by heating some discontinuous turns of a winding to different stable states respectively. The experimental test showed that the designed winding wire composite optical fiber sensor had a spatial resolution of 0.8 m (each light band was 3.2 m wide and consisted of four sampling points). For the continuously winded winding inside a transformer, this accuracy is sufficient for positioning the exact turn of local overheating.

D. FABRICATION OF DISTRIBUTED OPTICAL FIBER SENSOR INTEGRATED TRANSFORMER

The components of the DOFS integrated transformer system are shown in Figure 9. The optic fiber flange was sealed firmly on the transformer tank with the external optical extension cable connected to the data processing system for signal extraction. The system was manufactured in strict accordance with the conventional manufacturing process, which had passed the factory test of relevant industry standards, meeting the grid operation standards. This potently evidenced that the fiber optic sensor presented remarkable safeness and steadiness inside the transformer, and could be further utilized in real industrial applications.

IV. REALTIME HOTSPOT TRACING AND ONLINE TEMPERATURE MONITORING RESULTS

The temperature rise assay was carried out in accordance with the IEC 60076-7: 2018[11] standard, during which spatiotemporal temperature variations inside the transformer were detected in real-time using distributed optical fiber sensors.

The temperature distribution of the entire windings was directly and persistently monitored at the same time, as shown in Figure 10. The hotspots of the windings were also fairly close during the whole process, the trajectory of which was exhibited in Figure11.
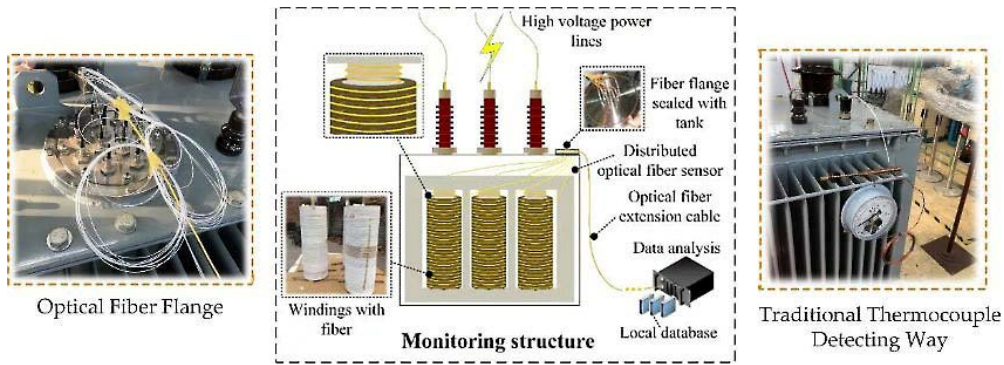
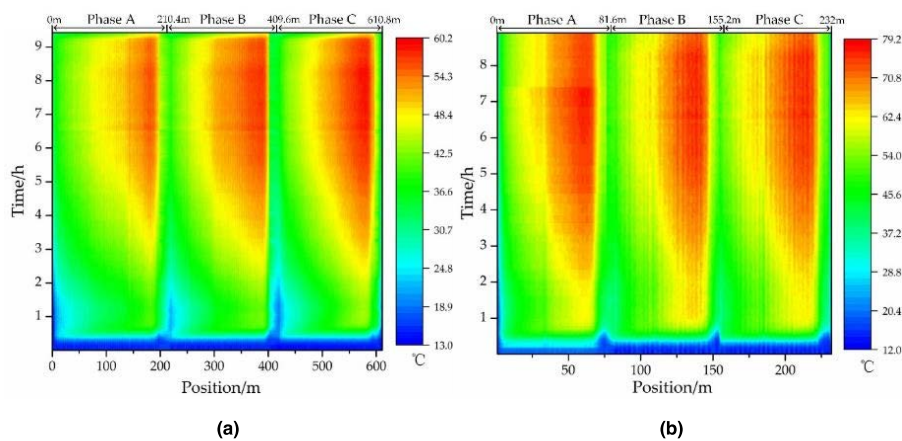**FIGURE 9.** Online thermal monitoring of optical fiber integrated power transformer.

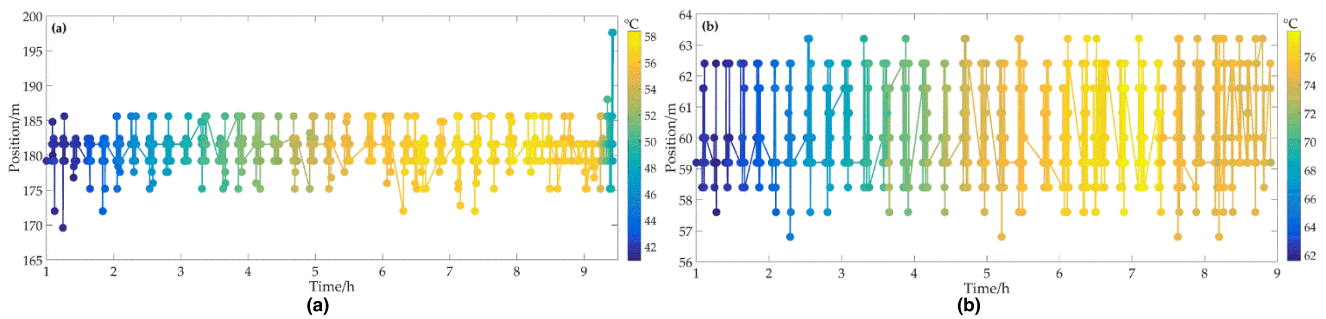**FIGURE 10.** Distributed temperature results for: (a) HV winding; (b) LV winding.

FIGURE 11. Hotspot track of phase A after 1h for (a) HV winding; (b) LV winding.

The entire temperature rise test was carried out by the short circuit approach, which lasted for approximately 9 hours, and there were 2 steps: adding the test current which was in correspondence to the total loss of the transformer, including the load loss and no-load loss (the first 8 h); adding the rating current which was in correspondence to the load loss of the transformer (the last 1 h). During this period, DFOS could realize the persistent monitoring and effective sensing of the winding temperature.

In general, there are two kinds of losses, or rather heat sources, in transformers, i.e., copper losses generated from the joule heat of the copper conductor and iron losses generated from magnetic hysteresis loss and the eddy current loss of the ferromagnetic material. As the name suggests, the first step of the temperature rise test was the application of both losses on windings (by increasing current to a level where the generated heat equaled the total heat of normal operation), while the following step reduced the current to the rated value.

For the three-phase windings, the optical fiber was winded uniformly and the total sensing length for each phase was also listed in Figure 10.

As shown in Figure 4, the fibers were uniformly wound helically along the winding surface, so the fiber length could be converted into the winding height for analysis (discussed in detail later). According to Figure 10(**a**), the high-voltage winding temperature of each phase displayed the incremental tendency with the increase of fiber length, but the temperature at the top of the winding didn't follow this trend, which might be induced by the comparatively good conditions for heat dissipation.

In addition, the hottest regions progressively appeared after we applied the total loss for 3 hours, which were phases A, B, and C, in correspondence to temperatures of about 50°C, 49°C, and 51°C. These regions were located at about 86%, 84%, and 85% of the winding height. As time passed, the relatively hotter regions started to expand, and at the end of the first step (8h), the hot region with a temperature above 54 °C (90 % of the highest temperature) occupied 79 %∼89 %, 66 %∼93 %, 66 %∼95 % of the winding height, respectively. The hotspots for phases A, B, and C during the whole process fluctuated at around 83 %∼88 %, 84 %∼89 %, and 85 %∼90 % of the winding height, respectively (Figure 11(**a**)).

Compared with the HV winding, the LV winding exhibited a greater temperature because of its greater current, as presented in Figure 10(**b**), and the temperature increased initially and afterward decreased with the fiber length. Moreover, the hotspot arose earlier than 1 hour after the application of total losses, and the part with a temperature value of 60 was mainly distributed at 73 %∼75 % of the winding height. The hot spot persistently spread to a larger area over time, and nearly half of the windings were over 71 °C (90 % of the highest temperature) at 8h. The hotspots for phases A, B, and C throughout the process fluctuated at 70 %∼76 %, 71 %∼75 %, and 70 %∼75 % of the height, respectively (Figure 11(**b**)).

The transformer studied in this paper adopted a layered winding structure (i.e., there wasn't any oil channel between every winding wire, as shown in Figure 3), and the temperature along the entire winding was uniform and continuous, and there was no sudden temperature jump. At the same time, since the optic fiber was spirally wound along the surface of the wire to form a winding-integrated sensor, the spatial position function of the three-phase sensing fiber could be established through the spiral equation according to the fiber length and the winding size (Figure 12), and the corresponding temperature data could be correlated with the spatial location based on it. Moreover, to achieve complete distributed temperature sensing, the temperature lying below the spatial resolution could be estimated by interpolation methods in the case of densely wound fibers.

The transformer studied in this paper adopted a layered winding structure (i.e., there was no oil channel between every winding wire, as shown in Figure 3), and the
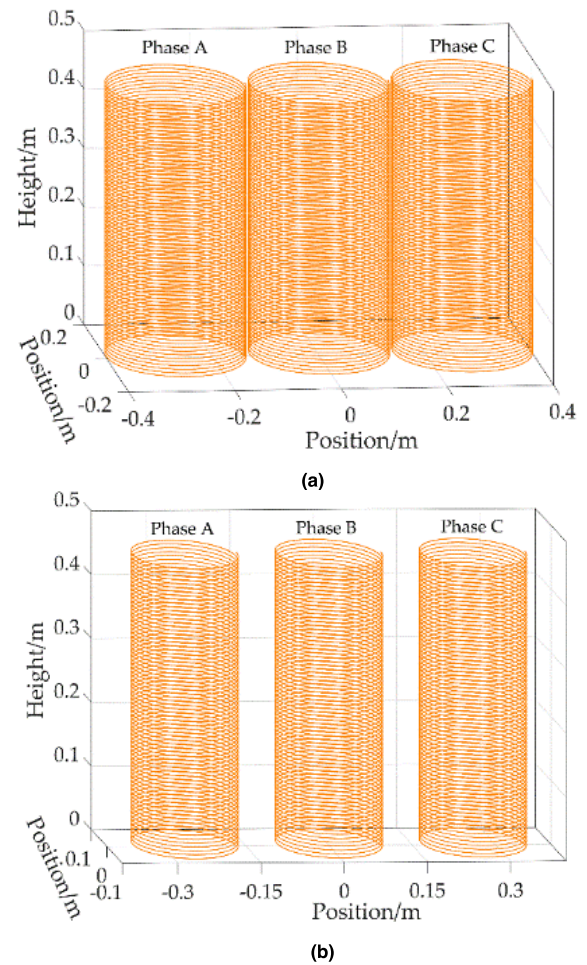

FIGURE 12. Spatial position function for three-phase sensing fibers of (a) HV winding; (b) LV winding.

temperature along the entire winding was uniform and continuous, and there was no sudden temperature jump. At the same time, since the optic fiber was spirally wound along the surface of the wire to form a winding-integrated sensor, the spatial position function of the three-phase sensing fiber could be established through the spiral equation according to the fiber length and the winding size (Figure 12), and the corresponding temperature data could be correlated with the spatial location based on it. Moreover, to achieve complete distributed temperature sensing, the temperature lying below the spatial resolution could be estimated by interpolation methods in the case of densely wound fibers.

By applying the distributed optical fiber sensors to the transformer online monitoring area, the actual temperature distribution inside the transformer could be obtained in a continuous distribution manner, and the hotspots could be closely tracked in real-time, which provided a new vision for power online monitoring and reliable data-based standards for the management of power transformers.

In addition, evaluating and analyzing the thermodynamic models of transformers based on the data obtained from distributed optical fibers can provide new perspectives and
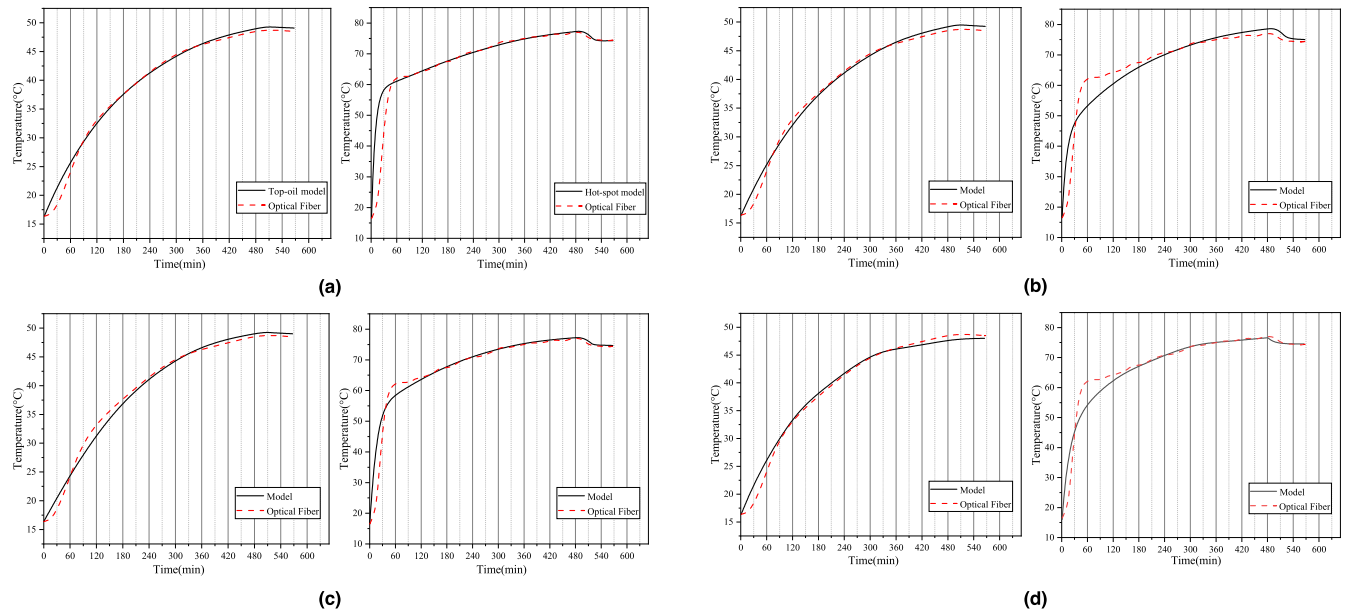
FIGURE 13. IEC TOT and HST model at (a), Swift TOT and HST model at (b), Susa TOT and HST model at (c), IEEE TOT and HST model at (d).

methods for analyzing their thermodynamic phenomena and comparing their strengths and weaknesses.

V. COMPARISON BETWEEN DISTRIBUTED OPTICAL FIBER SENSOR AND SEVERAL THERMAL MODELS

A. DYNAMIC COMPARISON CHART OF FOUR TYPICAL MODELS BASED ON DISTRIBUTED OPTICAL FIBER DATA

For the sake of describing the thermodynamic behaviors of transformers, certain classical modeling methods have been put forward, which can describe fairly intricate thermal transference circumstances based on simplified differential equations.

Based on the aforesaid analysis, it can be found that DOFS can realize the real-time and accurate monitoring of transformer HST. Since the sensing fibers were not arranged in all transformers, the accuracy of the existing transformer hotspot models was studied based on the test results, and the model prediction results were compared with DOFS test results.

When we compared and analyzed the hotspot data obtained by distributed optical fibers and dynamic models, we could not only further verify the correctness and accuracy of the hotspot tracking method using distributed optical fibers but could find the most suitable model to delineate the thermodynamic feature of the transformer. In this section, our team analyzed and compared four typical thermal models with the optical fiber data acquired from the temperature rise tests of a 200-KVA-ONAN-cooled unit and the hottest spot temperature data were derived from the low voltage winding.

The following figures show the comparisons between the TOT and HST of the IEC, Susa, Swift, and IEEE models and the fiber data.

Since the temperature rise test was divided into two stages, the total loss was applied to the transformer at the first stage. At this time, the test current was greater than the rated current. In the second stage, the rated current was applied to the transformer for 1 hour. Therefore, the TOT and HST of the latter part of the transformer would descend. As shown in the figure, at about 480 minutes, both the data of the four classical models and the temperature data measured by the fiber began to decline. Through the comparison and evaluation of the four top oil model diagrams, it can be seen that the model results and the optical fiber data exhibited a high degree of fitting in the transient and steady-state links, which was additionally the end result of a giant margin for the degree of oil temperature change.

It can be found from Figure 13(a) that in the transient part of the IEC HST model, the model data were higher than the optical fiber data, which might be due to the model's unthoughtful consideration of the temperature-varying oil viscosity, the influence of the driving force on oil viscosity and the hotspot heating rate in the case of a large load rate. In the steady-state part of the model, it can be seen that it fitted well with the fiber data, and the sensitivity of the model was also high when the load changed.

As presented in Figure 13(b), the estimated TOT rise of the Swift model coincided well with the data. Moreover, the transient temperature calculated in the HST model responded faster to the load, and the time required to reach the stable values of the TOT and HST was shorter. At the same time, there was a certain deviation between the estimated value of the HST and the optical fiber data, which was mainly reflected in the early transient process. It was related to the fact that the nonlinearity of the Swift model didn't completely offset

the influence of the viscosity and heat dissipation efficiency changes caused by oil temperature.

It can be determined from Figure 13(c) that Susa's HST model not only agreed well with the optical fiber data in the transient and steady-state parts, but had high accuracy and sensitivity in the process of altering with the load, which might be due to the fact that natural heat transfer and dynamic oil flow were included in the construction of the Susa model, with oil viscosity and temperature-dependent load loss as additional parameters. At the same time, the thermal resistance of the transformer was treated as a constant in the same way as the Swift model.

As shown in Figure 13(d), although the IEEE TOT model coincided well with the data, the accuracy of its HST data was not satisfactory in the transient aspect, which might be due to the overcompensation for the influence of oil viscosity. When the load changed, it could be considered that the change of the HST model was approximately exponential, which was associated with its unique algorithm and approximate data processing. Moreover, the IEEE model had an unique advantage in that the structure was almost linear, and the linear least squares could be effortlessly used and integrated into the monitoring system, which could adjust the transformer with a forced cooling system to enhance the accuracy of the model.

B. COMPARISON AND ANALYSIS

It is worthwhile to summarize and contrast the heat models and study the method of distributed optical fiber sensors. The following two diagrams show the comparison of TOT and HST data between the distributed optical fiber and four classical models.

From the comparison of the above four models and the optical fiber data, although the Susa model and IEC model exhibited great differences in structures, the temperature response curves calculated by the two models were similar to the optical fiber data. In order to evaluate the accuracy of the model and find the model with superior performance, this article calculated the root mean square error (RMSE) to compare and analyze the data obtained by the model and the optical fiber data set. The result is as follows:

The RMSE of the IEC, Susa, Swift, and IEEE models were 5.1039, 3.0766, 4.0267, and 3.1016, respectively.

It can be discovered that the RMSE of the Susa model was the smallest, which indicated that the fitting degree of the Susa model's data and the optical fiber data was the best and the error was the smallest. Moreover, the accurateness of the Susa model was greater in contrast to the other three models in Figure14 (b), whereas the structures of the calculation equations for the temperature in the Susa model were complex, which would limit their application in rapid engineering calculation.

Figure 14(b) reveals that there was a certain deviation between the dynamic temperature calculated by the Swift and IEEE models and the measured value. Relatively speaking, the former presented a larger error. According to [32], due to the structural defects of the Swift model, i.e., $\Delta\theta_{hr}$ was not
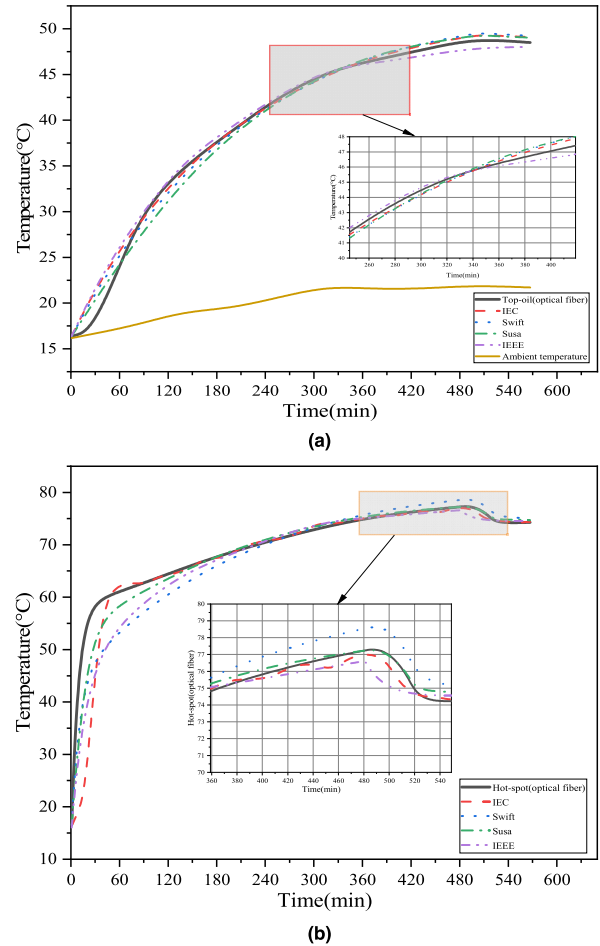

FIGURE 14. Four typical models, TOT model at (a); HST model at (b).

considered in the denominator when the time constant of the windings was estimated. The result was approximately twice the results of the other models, so the fitting results of the Swift model were poor. To sum up, despite certain shortcomings, Susa model is more suitable for the HST modeling in terms of accuracy, stability, and sensitivity.

VI. CONCLUSION

In this paper, a distributed optical fiber temperature detection system was established as per the principle of Raman scattering, and the optical fiber was applied to the transformer winding temperature detection, hot spot location tracking, and so on. The distributed optical fibers were fabricated in the double-winding oil-immersed transformer with a rated voltage of 35KV and a rated capacity of 200KVA in operation. The transformer prototype has passed the power grid operation test and factory test. By virtue of the DFOS system, the internal hotspot data could be obtained in real-time, including the temperature information and spatial information. Four kinds of thermodynamic models for the transformer (IEC, IEEE, Swift, and Susa) were constructed, and the data obtained by distributed optical fiber sensors were compared and analyzed based on the model results. The RMSE values

of different hotspot models were also calculated to find the optimal model.

The determination of the DFOS system and the optimal HST model has great significance and effect on the internal thermodynamic analysis of the transformer, real-time detection of winding temperature, hot spot tracking, and practical engineering applications. At the same time, the data obtained by optical fibers revealed the phenomena which is different from traditional theories. It is believed that this could provide other researchers with new directions and inspirations.

The relevant conclusions are as follows.

I. The as-designed optical fiber laying scheme can hold a steady status for the normal operation of transformers and exhibits satisfactory compatibility with transformer oil.

II. The optical fiber can effectively detect the real temperature of the windings due to its relatively small size and close contact with the wires. Hence, a spatiotemporally continuous temperature distribution can be obtained.

III. According to the experimental findings, the real-time temperature distribution of the transformer windings showed an increasing trend with the increase of height in all windings of all phases, apart from the top regions (with a decreasing trend), which might be due to the relatively good thermal conditions.

This new finding contradicts with the conventional wisdom that the hottest areas always arise at the top of windings, where heat tends to accumulate. However, it ignores the heat dissipation conditions that obviously exert great influences on temperature distribution, which can cause different shifts of hotspots according to our experiments and detection. Thereby, to build a more accurate calculation model, much deeper studies are warranted in the future.

IV. The actual hotspots of different windings inside the power transformer were persistently located and traced. They fluctuated at 83 %~88 %, 84 %~89 %, and 85 %~90 % of the high voltage winding height for phase A, B, and C, and they fluctuated at 70 %~76 %, 71 %~75 % and 70 %~75 % of the low voltage winding height for phases A, B, and C, respectively.

V. After calculation, the RMSE values of the four transformer hotspot models (IEC, Susa, Swift, and IEEE) were 5.1039, 3.0766, 4.0267, and 3.1016, respectively, which proved that the Susa model had the highest fitting degree and the strongest sensitivity. Through the comprehensive comparison and analysis of four classical models, the Susa model was determined as the best one, which was the most appropriate to model describe the dynamic thermal behaviors of power transformers.

VII. PATENTS

A. AUTHOR CONTRIBUTIONS

Conceptualization, R.D.; Methodology, R.D.; Validation, R.D. and X.F.; Formal analysis, R.D. and X.F.; Writing—original draft preparation, R.D.; Writing—review and editing, R.D. and X.F.; Visualization, R.D.; Supervision, X.F.;

Funding acquisition, X.F. All authors have read and agreed to the published version of the manuscript.

B. FUNDING

C. ABBREVIATION

The following abbreviations are used in this manuscript:

DFOS	Distributed optical fiber sensing
HST	Hottest-spot Temperature
TOT	Top-oil Temperature

REFERENCES

[1] S. S. M. Ghoneim, K. Mahmoud, M. Lehtonen, and M. M. F. Darwish, "Enhancing diagnostic accuracy of transformer faults using teaching-learning-based optimization," *IEEE Access*, vol. 9, pp. 30817–30832, 2021, doi: 10.1109/ACCESS.2021.3060288.

[2] M. Elsisi, M.-Q. Tran, K. Mahmoud, D. E. A. Mansour, M. Lehtonen, and M. M. F. Darwish, "Effective IoT-based deep learning platform for online fault diagnosis of power transformers against cyberattacks and data uncertainties," *Measurement*, vol. 190, Feb. 2022, Art. no. 110686. Accessed: Apr. 27, 2022. [Online]. Available: http://www.sciencedirect.com/science/article/pii/S0263224121015475

[3] S. A. Ward, A. El-Faraskoury, M. Badawi, S. A. Ibrahim, and M. Darwish, "Towards precise interpretation of oil transformers via novel combined techniques based on DGA and partial discharge sensors," *Sensors*, vol. 21, no. 6, p. 2223, 2021, doi: 10.3390/s21062223.

[4] F. Torriano, M. Chaaban, and P. Picher, "Numerical study of parameters affecting the temperature distribution in a disc-type transformer winding," *Appl. Therm. Eng.*, vol. 30, nos. 14–15, pp. 2034–2044, 2010, doi: 10.1016/j.applthermaleng.2010.05.004.

[5] M. M. Islam, G. Lee, and S. N. Hettiwatte, "A review of condition monitoring techniques and diagnostic tests for lifetime estimation of power transformers," *Electr. Eng.*, vol. 100, no. 2, pp. 581–605, Jun. 2018, doi: 10.1007/s00202-017-0532-4.

[6] A. J. Amalanathan, R. Sarathi, S. Prakash, A. K. Mishra, R. Gautam, and R. Vinu, "Investigation on thermally aged natural ester oil for real-time monitoring and analysis of transformer insulation," *High Voltage*, vol. 5, no. 2, pp. 209–217, Apr. 2020, doi: 10.1049/hve.2019.0178.

[7] A. M. Alshehawy, D.-E.-A. Mansour, M. Ghali, M. Lehtonen, and M. M. F. Darwish, "Photoluminescence spectroscopy measurements for effective condition assessment of transformer insulating oil," *Processes*, vol. 9, no. 5, p. 732, Apr. 2021, doi: 10.3390/pr9050732.

[8] Y.-M. Zhu, Y. Gong, and Z.-G. Yang, "Failure analysis on over-temperature combustion of transformers in 4 MW offshore wind turbines," *Eng. Failure Anal.*, vol. 96, pp. 211–222, Feb. 2019, doi: 10.1016/j.engfailanal.2018.10.005.

[9] J. M. Weed, "The temperature gradient in oil immersed transformers," *Proc. Amer. Inst. Elect. Eng.*, vol. 30, no. 1, pp. 119–138, Jan. 1911, doi: 10.1109/PAIEE.1911.6660333.

[10] *Power Transformers—Part 7: Loading Guide for Mineral-Oil-Immersed Power Transformers*, Standard IEC 60076-7, 2018. Accessed: Feb. 8, 2022. [Online]. Available: https://global.ihs.com/doc_detail.cfm?item_s_key=00470232

[11] D. J. Tylavsky, Q. He, G. A. McCulla, and J. R. Hunt, "Sources of error in substation distribution transformer dynamic thermal modeling," *IEEE Trans. Power Del.*, vol. 15, no. 1, pp. 178–185, Jan. 2000, doi: 10.1109/61.847248.

[12] M. F. Lachman, P. J. Griffin, W. Walter, and A. Wilson, "Real-time dynamic loading and thermal diagnostic of power transformers," *IEEE Trans. Power Del.*, vol. 18, no. 1, pp. 142–148, Jan. 2003, doi: 10.1109/TPWRD.2002.803724.

[13] T.-W. Park and S. H. Han, "Numerical analysis of local hot-spot temperatures in transformer windings by using alternative dielectric fluids," *Electr. Eng.*, vol. 97, no. 4, pp. 261–268, Dec. 2015, doi: 10.1007/s00202-015-0335-4.

[14] G. Liu, Z. Zheng, X. Ma, S. Rong, W. Wu, and L. Li, "Numerical and experimental investigation of temperature distribution for oil-immersed transformer winding based on dimensionless least-squares and upwind finite element method," *IEEE Access*, vol. 7, pp. 119110–119120, 2019, doi: 10.1109/ACCESS.2019.2937548.

[15] J. Smolka, A. J. Nowak, and L. C. Wrobel, "Numerical modelling of thermal processes in an electrical transformer dipped into polymerised resin by using commercial CFD package fluent," *Comput. Fluids*, vol. 33, nos. 5–6, pp. 859–868, Jun. 2004, doi: 10.1016/j.compfluid.2003.06.008.

[16] J. Gastelurrutia, J. C. Ramos, G. S. Larraona, A. Rivas, J. Izagirre, and L. del Río, "Numerical modelling of natural convection of oil inside distribution transformers," *Appl. Thermal Eng.*, vol. 31, no. 4, pp. 493–505, Mar. 2011, doi: 10.1016/j.applthermaleng.2010.10.004.

[17] J. R. D. Silva and J. P. A. Bastos, "Online evaluation of power transformer temperatures using magnetic and thermodynamics numerical modeling," *IEEE Trans. Magn.*, vol. 53, no. 6, pp. 1–4, Jun. 2017, doi: 10.1109/TMAG.2017.2666602.

[18] A. B. L. Ribeiro, N. F. Eira, J. M. Sousa, P. T. Guerreiro, and J. R. Salcedo, "Multipoint fiber-optic hot-spot sensing network integrated into high power transformer for continuous monitoring," *IEEE Sensors J.*, vol. 8, no. 7, pp. 1264–1267, Jul. 2008, doi: 10.1109/JSEN.2008.926926.

[19] A. Y. Arabul, F. K. Arabul, and I. Senol, "Experimental thermal investigation of an ONAN distribution transformer by fiber optic sensors," *Electr. Power Syst. Res.*, vol. 155, pp. 320–330, Feb. 2018, doi: 10.1016/j.epsr.2017.11.007.

[20] A. Barrias, J. R. Casas, and S. Villalba, "A review of distributed optical fiber sensors for civil engineering applications," *Sensors*, vol. 16, no. 5, p. 748, 2016, doi: 10.3390/s16050748.

[21] M. Djamali and S. Tenbohlen, "Hundred years of experience in the dynamic thermal modelling of power transformers," *IET Gener., Transmiss. Distrib.*, vol. 11, no. 11, pp. 2731–2739, Aug. 2017, doi: 10.1049/iet-gtd.2016.1321.

[22] Y. Liu, Y. Tian, X. Fan, Y. Bu, and B. Wang, "Detection and identification of transformer winding strain based on distributed optical fiber sensing," *Appl. Opt.*, vol. 57, no. 22, p. 6430, Aug. 2018, doi: 10.1364/AO.57.006430.

[23] C. V. Raman and K. S. Krishnan, "A new type of secondary radiation," *Nature*, vol. 121, no. 3048, pp. 501–502, 1928, doi: 10.1038/121501c0.

[24] A. M. Zheltikov, "Nano-optical dimension of coherent anti-Stokes Raman scattering," *Laser Phys. Lett.*, vol. 1, no. 9, pp. 468–472, Sep. 2004, doi: 10.1002/lapl.200410099.

[25] L. Meng, M.-S. Jiang, Q.-M. Sui, and D.-J. Feng, "Optical-fiber distributed temperature sensor: Design and realization," *Optoelectron. Lett.*, vol. 4, no. 6, pp. 415–418, Nov. 2008.

[26] G. Swift, T. S. Molinski, and W. Lehn, "A fundamental approach to transformer thermal modeling. I. Theory and equivalent circuit," *IEEE Trans. Power Del.*, vol. 16, no. 2, pp. 171–175, Apr. 2001, doi: 10.1109/61.915478.

[27] G. Swift, T. S. Molinski, R. Bray, and R. Menzies, "A fundamental approach to transformer thermal modeling. II. Field verification," *IEEE Trans. Power Del.*, vol. 16, no. 2, pp. 176–180, Apr. 2001, doi: 10.1109/61.915479.

[28] D. Susa, M. Lehtonen, and H. Nordman, "Dynamic thermal modelling of power transformers," *IEEE Trans. Power Del.*, vol. 20, no. 1, pp. 197–204, Jan. 2005, doi: 10.1109/TPWRD.2004.835255.

[29] *IEEE Guide for Loading Mineral-Oil-Immersed Transformers and Step-Voltage Regulators—Redline*, IEEE Standard C57.91-2011 (Revision of IEEE Standard C57.91-1995, 2012. Accessed: Feb. 21, 2022. [Online]. Available: http://ieeexplore.ieee.org/document/6197686

[30] S. B. Paramane, W. Van Der Veken, A. Sharma, and J. Coddé, "Effects of oil leakage on thermal hydraulic characteristics and performance of a disc-type transformer winding," *Appl. Thermal Eng.*, vol. 98, pp. 1130–1139, Apr. 2016.

[31] Y. Liu, S. Jiang, X. Fan, and Y. Tian, "Effects of degraded optical fiber sheaths on thermal aging characteristics of transformer oil," *Appl. Sci.*, vol. 8, no. 8, p. 1401, Aug. 2018, doi: 10.3390/app8081401.

[32] O. A. Amoda, D. J. Tylavsky, G. A. McCulla, and W. A. Knuth, "Acceptability of three transformer hottest-spot temperature models," *IEEE Trans. Power Del.*, vol. 27, no. 1, pp. 13–22, Jan. 2012, doi: 10.1109/TPWRD.2011.2170858.

RAN DUAN is currently pursuing the B.S. degree with North China Electric Power University. He is also working with the Hebei Provincial Key Laboratory of Power Transmission Equipment Security Defense. His research interests include transformer and optical fiber sensors.

• • •